Progress in Organic Coatings 174 (2023) 107291

Contents lists available at ScienceDirect

Progress in Organic Coatings

journal homepage: www.elsevier.com/locate/porgcoat

Surface modification of 316L stainless steel with multifunctional locust gum/polyethylene glycol-silver nanoparticles using different coating methods

Gizem Karabulut [a,*], Nuray Beköz Üllen [a], Esin Akyüz [b], Selcan Karakuş [c]

[a] Istanbul University-Cerrahpasa, Department of Metallurgical and Materials Engineering, 34320 Istanbul, Turkey
[b] Istanbul University-Cerrahpasa, Faculty of Engineering, Department of Chemistry, Analytical Chemistry Section, 34320 Istanbul, Turkey
[c] Istanbul University-Cerrahpasa, Faculty of Engineering, Department of Chemistry, Physical Chemistry Section, 34320 Istanbul, Turkey

ARTICLE INFO

Keywords:
Ag NPs
Surface modification
Nanotechnology
Antibacterial activity
Corrosion resistance

ABSTRACT

316 L stainless steel (SS316L) has attracted significant attention in both implantable and non-implantable medical devices for its biocompatibility. However, bacterial adhesion on the surface of SS316L and corrosion after contact with body fluids challenge its usability as a bioimplant. It is therefore necessary to improve the antibacterial and anticorrosion properties of SS316L. One of the most effective ways to achieve this is to deposit a protective metal nanoparticles-based coating on the surface of SS316L. In this study, organic Locust Gum/polyethylene glycol-silver nanoparticles (Loc/PEG-Ag NPs) were synthesized with sonochemical method, and characterized to determine their morphology, crystal structure, chemical functional groups, and antioxidant capacity. The synthesized Ag NPs were coated on SS316L with drop casting and airbrush spray coating methods. The morphological characteristics, superficial properties, antibacterial activity, and corrosion resistivity of the surface modified SS316L were evaluated. A multifaceted investigation was performed to understand the surface characteristics and to improve the productivity of the Ag NPs coating on the metallic surface. The antioxidant capacities of the spherical-shaped Loc/PEG-Ag NPs with an average size of 10 to 50 nm were found to be 17.90 ± 0.50 and 20.47 ± 0.19 mmol Trolox equivalent (TE)g^{-1}, respectively. The airbrush spray coating treatment significantly improved the surface properties of the substrate due to the formation of a thin layer (8.47 μm), affecting interactions between Ag NPs and substrates. The Ag NPs coated SS316L demonstrated high antibacterial activity against *E. coli* and *S. aureus* at a diameter of 28 mm and 19 mm, respectively. Compared with the bare substrate, the corrosion resistance of the surface modified SS316L is improved. The results illustrated the importance of surface nano-modification in attaining favorable antibacterial and anticorrosive performance. It is believed that the Loc/PEG-Ag NPs coated SS316L could be a promising multifunctional (i.e., uniform coating +biological activity +corrosion resistance) nanoplatforms in biomedical applications.

1. Introduction

Applications of nanotechnology have been preferred in a variety of fields, such as electronics [1], textiles [2], environmental applications [3], medicine [4], and materials science [5]. Due to the small size of the nanoparticles (NPs), the increased effective surface area allows them to acquire unique properties [6]. In this way, multifunctional metal-based NPs are used to improve the surfaces of many materials, such as textiles [7,8], polymers [9], and metals [10]. In particular, metallic NPs-based coatings on metallic substrates have been a frequently studied subject in recent years [11–19]. Multifunctional NPs-based coatings are in a very important position in terms of the coating of metallic biomaterials to cope with bioinert behavior [20], corrosion [21,22], mechanical [22], and biofilm formation problems [21,23,24], and control of drug release systems [21,23], etc. Multifunctional nanobiocomposite coatings have come to the fore to solve these problems and improve the surface properties of metallic biomaterials [25]. Recently, silver nanoparticle (Ag NPs)-based coatings have shown great potential as an extremely important and effective solution to deal with pathogen-related problems. As known, silver has broad-spectrum activity against many

* Corresponding author.
E-mail addresses: gizem.karabulut@iuc.edu.tr (G. Karabulut), nbekoz@iuc.edu.tr (N. Beköz Üllen), kondakci@iuc.edu.tr (E. Akyüz), selcan@iuc.edu.tr (S. Karakuş).

https://doi.org/10.1016/j.porgcoat.2022.107291
Received 24 May 2022; Received in revised form 19 October 2022; Accepted 23 October 2022
0300-9440/© 2022 Elsevier B.V. All rights reserved.

pathogens such as microbes, fungi, bacteria, and viruses [26–28]. Furthermore, Ag NPs can be preferred in cosmetics, food, textiles, and many other applications with their superior antimicrobial, antifungal, antibacterial, and antioxidant properties provided by their high surface area [29]. In addition to these antipathogenic properties, Ag NPs can be preferred in metal coating applications with their thermal stability, electrical conductivity, photocatalytic activity, and corrosion properties. The main purpose of the coating is the use of nanoscale thin films applied to the surface of the materials that improve the surface functionality (antibacterial, anticorrosive, antifouling, etc.) of the substrate material [30,31].

Generally, coating methods such as dip [30,32], sol-gel [33], plasma-enhanced chemical vapor deposition [34] and electro-deposition [35] were used in the studies on Ag NPs-based coatings of metallic substrates. These methods are generally difficult, expensive, and long-term processes. Today, as a result of the increase and development in industrialization and the escalation of competition, fast, cost-effective, and easy-to-apply methods are preferred in mass production. Therefore, the purpose of this study is to homogeneously coat the Ag NPs synthesized with an eco-friendly green chemistry technique on the SS316L surface with easy, cost-effective, and fast methods. Firstly, Ag NPs were synthesized using the sonochemical method in this study. In this method, the formation of NPs is carried out by acoustic cavitation using ultrasonic sound waves [36]. It is a green synthesis method to reduce Ag ions to form Ag NPs without the use of chemical reducing or hazardous stabilizing agents [37]. Ag NPs' proclivity to agglomerate and collapse in liquid is a significant barrier to their application [38]. In the present study, locust bean gum (Loc) and polyethylene glycol (PEG) were used as stabilizing and reducing agents to overcome this obstacle. Loc is a natural polymer. It is used in various industries, especially in the food and pharmaceutical industries, due to its biocompatibility, edibility, adhesiveness, and thickening properties [39]. PEG is a biocompatible, green, and cost-effective synthetic non-toxic multifunctional polymer with a uniform chain structure that can be used in many areas for thickening, softening, and dissolving purposes [40–42]. Then, the Loc/PEG-Ag NPs were coated on the SS316L surface using drop casting and airbrush spray coating techniques. The drop casting technique is the coating of the solution as droplets on the surface with a pipette [43,44]. The airbrush spray technique is commonly used for coating solar panels or electrodes. The coating is carried out by spraying the solution through a nozzle at a certain pressure [43,44]. It is an easy-to-apply, fast, cost-effective, and green process in both techniques [44].

SS316L is commonly used in biomedical applications due to its high strain properties, ease of availability, and low cost [45,46]. In addition to the improved corrosion properties with Ni and Mo, these properties are increased with low carbon content [45]. SS316L is an austenitic stainless steel and is preferred in biomedical applications due to its high toughness, hardenability by heat treatment, machinability, and non-magneticity [45]. However, since SS316L is bioinert with tissues, can be corroded by contact with body fluid as pitting or crevice corrosion, and pathogens can grow on their surfaces, surface improvement is being studied with various coatings to overcome these problems. The coating consists of a surface modification process involving the addition of functional materials that give the product the desired properties [47]. The functionalized surface showed improved properties of SS316L, including the aforementioned properties, but bacterial infection is still the main obstacle. Ag NPs-based coatings on metallic surfaces due to their highly superior properties as an antibacterial agent have been of great interest to researchers in recent years and have recently received much attention in the literature. Zhang et al. coated the polytetrafluoroethylene (PTFE) layer on SS316L using a sol-gel based dip coating method, then immobilized Ag NPs on the surface and thus obtained the antibacterial nanocomposite structure on stainless steel [10]. Jothi et al. synthesized novel *Phyllanthus niruri* leaf extract-based Ag NPs in siloxane matrix (SiO_2 @ P.niruri-Ag NPs) and showed their antibacterial and corrosion-resistant surface by coating them on 304 stainless steel [33]. Abdulsada and Hammood used the electrophoretic deposition method to coat hydroxyapatite and Ag NPs on 2507 duplex stainless steel [35]. Qian et al. performed a multi-layer surface coating with polydopamine (PDA) and Ag NPs on SS316L in order to impart properties such as superhydrophilic, antibacterial, and corrosion resistance [48]. Up to date, only one previous research report on the Ag NPs-based coating on SS316L was studied by airbrush spray technique. Aminatun et al., synthesized the Ag NPs using the chemical reduction method and coated the Ag NPs-gelatin layer on SS316L using the airbrush spray technique [49]. As a result, nanotechnology can improve the topological structure of metallic surfaces by adding nanomaterials (NMs) or creating nanoscale surfaces. A summary and discussion of the types and properties of modified NMs to metallic surfaces, technical modification schemes, and nanomodified biological effects are urgently needed. The creation of nano-modified surfaces to control and improve the corrosive effects and antibacterial properties of metallic surfaces will facilitate the application of metals in medical fields [50]. Since the industrial studies focus on improving the surface properties of the coating, this study aims to produce a guideline and achieve the as-mentioned goals.

By investigating the anticorrosive and antibacterial properties of the superficially modified SS316L with Locust/PEG-Ag NPs organic nanostructure, the current study aimed to fill a knowledge gap in the literature. To the best of our knowledge, the coating of the Locust/PEG-Ag NPs on the SS316L with airbrush spray coating was the first study in this field. In this study, novel Loc/PEG-Ag NPs showed greatly enhanced biological performance using a combination of biomedical engineering and materials science-based strategies, and the formation of a layer of multifunctional Loc/PEG-Ag NPs on the surface of the SS316L using a simple and economical airbrush spray method seemed to play a crucial role in the surface property. Furthermore, this study provided new insight into the antioxidant, antibacterial, and corrosion resistance of synthesized Loc/PEG-Ag NPs and Loc/PEG-Ag NPs coated SS316L surfaces with multifunctional biological and chemical properties and paved the way toward better satisfying clinical needs. The obtained results emphasize that Ag NPs coated surfaces show antibacterial activity and anticorrosion properties, and these coatings can be used for the production of coated surfaces used in sensitive environments such as the medical and food industries.

2. Materials and methods

2.1. Materials

Polyethylene glycol 400 (PEG400) (molecular weight: 400 kDa) was obtained from Fluka (Switzerland). Locust bean gum (*Ceratonia siliqua* seeds), sodium hydroxide (NaOH) (molecular weight: 40.00 g/mol), ethanol (EtOH), copper(II) chloride, sodium dihydrogen phosphate, hydrogen peroxide solution (H_2O_2), 2,2-diphenyl-1-picrylhydrazyl (DPPH), 2,2′-azino-bis(3-ethylbenzothiazoline-6-sulfonic acid) diammonium salt (ABTS), and peroxidase from horseradish (HRP) were obtained from Sigma Aldrich Company (Germany). Ammonium acetate (NH_4Ac) and disodium hydrogen phosphate were supplied from Riedel–de Haën (Seelze, Germany). Silver nitrate ($AgNO_3$) (EMSURE® ACS, ISO, Reag. Ph Eur) was obtained from Merck Company (Germany). All chemicals were analytical grade and used as received without further purification.

2.2. Preparation of Loc/PEG-Ag NPs

1.0 g of Loc polymer matrix was dissolved in 250 mL of distilled water, kept in the dark for 1 day, and stirred at room temperature. At 25 °C, 12.5 mL of PEG and the Loc solution were mixed for 10 min. 0.84 g of $AgNO_3$ was dissolved in 500 mL of distilled water and added to the Loc/PEG blend. The solution was stirred at 25 °C for 10 min. 0.01 M of NaOH was slowly added to the Loc/PEG-$AgNO_3$ solution. The viscosity of the Loc/PEG-$AgNO_3$ solution were measured with viscometer (AND

Table 1
Chemical composition of SS316L (wt%).

C	Si	Mn	Ni	Cr	Mo	Cu	S	P	N	Fe
0.014	0.437	1.317	10.091	16.581	2.048	0.326	0.024	0.025	0.041	Balance

Weighing Viscometer SV 100 Model). The viscosity was measured to be 338 cP (pH:7.4 and 25 °C). The sample was sonicated for 10 min at 45 % amplitude frequency at room temperature (25 °C) and filtered using a sterile syringe filter (0.22 μm of pore size).

2.3. Preparation of Loc/PEG-Ag NPs coated SS316L substrates

SS316L obtained from Birçelik Company (Istanbul, Turkey) in the form of a bar with a length of 1 m was used as the substrate material. The chemical content of SS316L is given in Table 1. The values are taken from the technical inspection certificate of the company. The SS316L bar was sliced into 2 mm of thickness and 25 mm in diameter with a computer numerical control (CNC) machine (YouJi Machine Industrial Co. Ltd.) with X and Z axes at 550 mm machining volume and 3000 rpm in a dry condition without any coolant to obtain disc form. The parameters of the cutting process are presented in Table 2.

Table 2
The parameters of the cutting process.

Tool holder	PDJL 2020 K15
Insert	DNMG 150608 PM 1525
Cutting speed (m/min)	10
Feed (mm/rev)	0.25
Depth of cut (mm)	1.0

Before starting the coating process, the discs were sonicated for 10 min in ethanol and dried for 10 min at 60 °C in the oven. Drop casting was performed by using a pasteur pipette. 1.5 mL was taken from the solution with the pipette and dripped on the sample surface. Airbrush spray coating was performed by using an airbrush compressor kit (piston type, model number: AS186). The nozzle diameter of the spray gun is 0.2 mm. The prepared Loc/PEG-Ag NPs solution was transferred into the container, and the solution was sprayed onto the SS316L substrates. Spraying was carried out at 3 bar pressure for 4 s at a 75 mm distance. To prevent the sprayed solution from spreading around and to ensure that it is sprayed on the steel surface from an equal distance, a plastic pipe with a diameter of 28 mm was used. Following the coating process, the coated samples are oven dried for 1 h at °C. The schematic view of the experimental steps of the coating processes was given in Fig. 1.

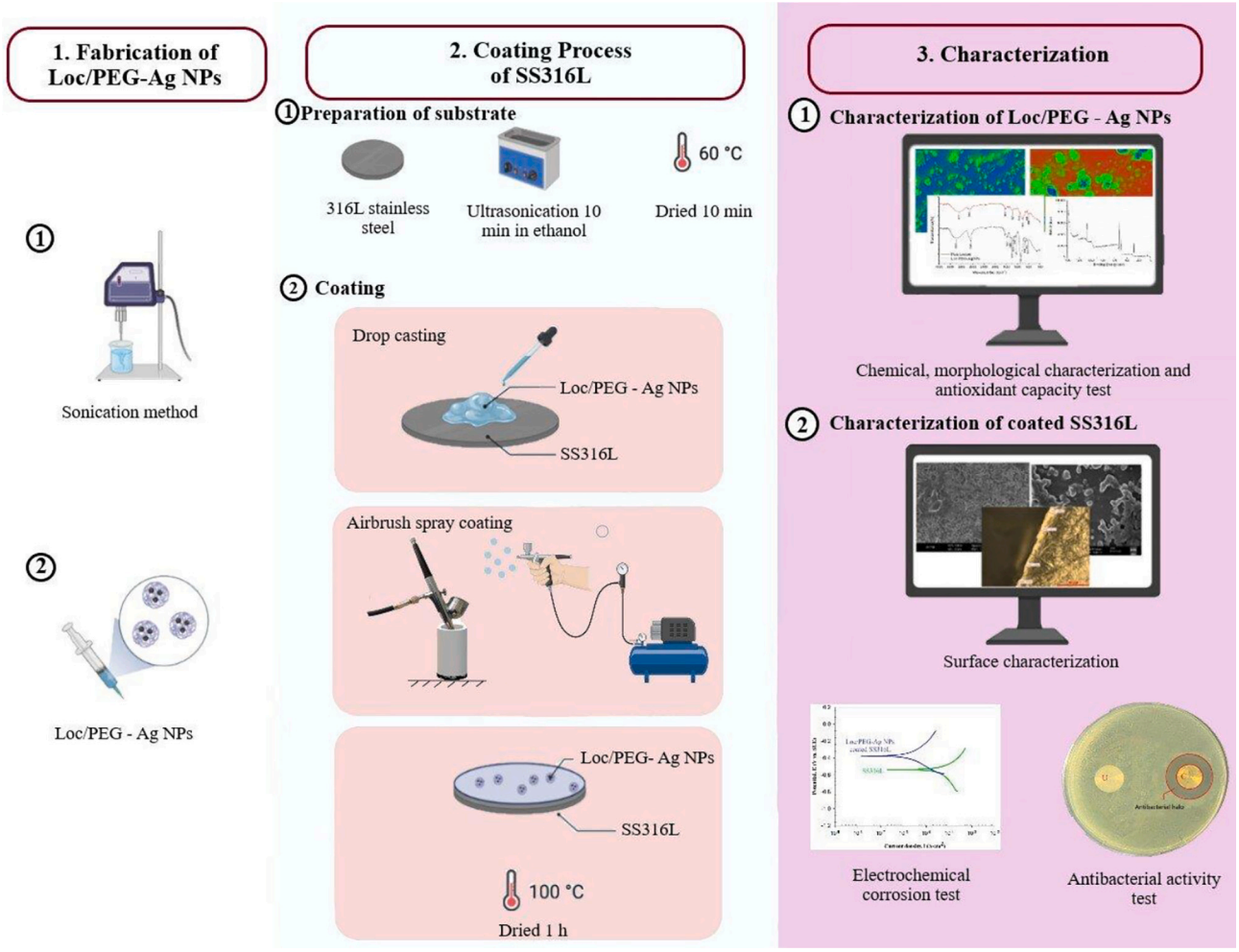

Fig. 1. Experimental steps of the coating processes.

2.4. Material characterization

In this study, scanning electron microscopy (SEM), energy dispersive X-ray spectrometry (EDS), transmission electron microscope (TEM), ultraviolet visible spectrophotometry (UV–Vis), Fourier transform infrared (FTIR) spectroscopy, X-ray diffraction (XRD), and X-ray photospectrometer (XPS) were used to characterize the synthesized multifunctional nanobiocomposite. An Agilent Cary 100 UV–Vis spectrophotometer (Santa Clara, CA, United States) was used for absorbance measurements in the antioxidant test. A select bioproducts vortexer was used to stir incubation solutions. Different techniques, such as optical microscopy, SEM, surface roughness, and profilometer techniques, were used to determine the surface and morphological structure characterization of the superficially modified SS316L.

The morphology and topography of the pure Loc, synthesized Loc/PEG-Ag NPs, and coated samples were characterized by SEM/EDS with a Zeiss-Sigma 300 device. The surface morphology and particle size of Loc/PEG-Ag NPs were determined by TEM in a high vacuum mode at 100 kV with Hitachi High Tech HT7700. The absorbances of the Loc/PEG-Ag NPs solution were measured using a double-beam UV–Vis spectrophotometer (T + 80 model, PG Instrument) with UVWin 5 Software. The Perkin Elmer (Spectrum Two model) was used to determine the functional groups of the pure Loc and Loc/PEG-Ag NPs in the 4000–400 cm^{-1} frequency range with a resolution of 4 cm^{-1} and 8 scans. The crystalline structures of the Loc/PEG-Ag NPs were measured by XRD with Cu-Kα radiation from 10° to 80° at 40 kV and 15 mA with the Rigaku D/Max2200/PC device. The elemental composition and chemical properties of the coating solution were investigated by XPS analysis using a Specs-Flex device with Al-Kα radiation. An optical microscope was used to examine the cross-sectional view of the coated parts and the coating thickness and the distribution of the coating on the surface. Samples were prepared by metallographic methods to obtain images with color contrast in the optical microscope and to view the coatings. For microstructural analysis, the parts were electrolytically etched in a solution with a 30 % NaOH-distilled water composition for 5 s, and for coating examination, the parts were electrolytically etched in a solution with a composition of 5 % oxalic acid-distilled water for 8 s. After samples were cleaned with alcohol and dried, metallographic and coating properties examinations were conducted with a Nikon brand MA100 model optical microscope. The surface roughness of uncoated and coated samples was determined with the Mitutoyo brand Surftest SJ-210 model device. The distribution and thickness of the coating on the surface were examined using a Kla Tencor Stylus Profiler P7 profilometer device. All images of the Ag NPs were carried out for determination of differences in color (RGB) (red-green-blue) distribution by a color histogram method (ImageJ 1.51q). The crystalline size of the prepared Loc/PEG-Ag NPs was calculated by the Debye-Scherrer Equation (Eq. (2.1)).

$$D_p = \frac{0.94.\lambda}{\beta.cos\,\theta} \tag{2.1}$$

where λ: X-ray wavelength (0.15406), β: full width at half maximum (FWHM), D: crystallite size diameter, and θ: Bragg's diffraction angle obtained from 2 Theta (θ).

2.5. Detection of total antioxidant capacity (TAC) assay

TAC of Loc/PEG-Ag NPs was determined using the spectrophotometric cupric ion reducing antioxidant capacity (CUPRAC) method and the 2,2′-azino-bis(3-ethylbenzothiazoline-6-sulphonate) (ABTS)/horseradish peroxidase (HRP) method in this study.

2.5.1. CUPRAC assay

The TAC of the antioxidants in the sample was based on reducing the Cu^{2+} to Cu^{1+} at 450 nm (absorbance measurement) [51]. The reagent solutions were prepared as follows: 10 mM of $CuCl_2$ and 1.0 M of NH_4Ac (pH: 7.0) solutions were dissolved in distilled water. 7.5 mM of neocuproine (Nc) solution was dissolved in absolute ethanol (EtOH). In the procedure of the assay, 1 mL of each Cu(II), Nc, and NH_4Ac buffer solutions were mixed in a test tube, and a 50 μL sample solution was added to the mixture. The total volume was adjusted to 4.1 mL with distilled water and incubated for 30 min at a constant temperature (25 °C) after the vortexing of all tubes. Then, absorbance values of all samples were recorded against a reagent blank at 450 nm. The TAC of Loc/PEG-Ag NPs (mmol TE g^{-1} dry sample) was calculated by using the calibration curve (absorbance vs. concentration of trolox standard) (CUPRAC assay: $\varepsilon_{TR} = 16{,}700\ Lmol^{-1}\ cm^{-1}$).

2.5.2. ABTS/HRP assay

The reagent solutions were prepared as follows: 4.0 mM of ABTS solution, 0.12 mM of hydrogen peroxide (H_2O_2) solution, and 0.024 mM of HRP solution were prepared in phosphate-buffered saline (PBS) (pH: 7.4). The method reported by Arnao et al. was partially modified with reagent amounts and duration times. In a test tube, 1 mL of ABTS (4.0 mM) [52], 1 mL of HRP (0.024 mM), and 1 mL of H_2O_2 (0.12 mM) solutions were mixed. The solution was kept for 5 min in the dark medium without any shaking to stabilize the solution due to the formation of ABTS radicals ($ABTS^{\bullet+}$). Finally, 50 μL of the Loc/PEG-Ag NPs sample was added (the total volume was adjusted to 4 mL with distilled water), vortexed, and kept for 5 min in the dark medium. Absorbance values of the sample were recorded at 10th min at 730 nm (reference: PBS solution, pH: 7.4). The difference in absorbance (ΔA) was calculated by the absorbance of the sample solution and the blank radical solution. The total antioxidant capacity (unit: mmol TE g^{-1} dry sample) of the Loc/PEG-Ag NPs sample was calculated using the calibration curve (absorbance vs. concentration of TR standard) ($\varepsilon_{TR} = 22{,}000\ Lmol^{-1}\ cm^{-1}$). The experiments of spectrophotometric methods were carried out at least three times, and descriptive statistical analyses were performed using Excel software (Microsoft Office 2016) to calculate the mean and the standard error of the mean. The results were presented as mean values with standard deviations (SD; $n = 3$).

2.6. Antibacterial assay

In this study, the antibacterial effect of the Loc/PEG-Ag NPs coated surface was investigated against to the gram-negative bacteria *Escherichia coli* (*E. coli*) and the gram-positive bacteria *Staphylococcus Aureus* (*S. aureus*) with agar well diffusion method. Firstly, *E. coli* and *S. aureus* bacteria were cultured overnight in a 12 mL plastic culture tube. Then, fresh culture was started in plastic culture tubes at a dilution of 1:500. When the starting fresh culture reached OD_{600}, 75 μL of *E .coli* and *S. aureus* cultures were added to Tryptic Soy Broth (TSB)-agar medium petri dishes separately. Afterward, the bacterial cultures were spread over the entire surface with a sterile spreader. After being spread, the plates were incubated for 20 min at 27 °C. After incubation, coated and uncoated samples were carefully replaced on the TSB-agar surface with sterile forceps. The uncoated and coated with the airbrush spray coating method samples with a diameter of 14 mm were used for the antibacterial test. Finally, the petri dishes were taken to the incubator and incubated at 37 °C for 24 h. After incubation, the zones of inhibition (ZOI) formed

around the samples were measured with the help of a ruler.

2.7. Electrochemical corrosion test

Electrochemical corrosion analysis was carried out on the bare and Loc/PEG-Ag NPs coated SS316L in the Ringer's solution using a potentiostat (Interface 1000 Potentiostat, Gamry, USA) controlled by a computer. Ringer's solution (pH: 7) was prepared with two Ringer's Tablets (Merck Company, Germany) in 1000 mL of distilled water. The conventional three-electrode system was used for corrosion measurements. In the system, samples were used as a working electrode, high density graphite as a counter electrode, and saturated calomel electrode (SCE) as a reference electrode. Data analysis was performed with software (Framework and Echem Analyst Gamry). The samples were prepared by mounting them in the epoxy resin and then being connected to a copper wire. The volume of the corrosion test cell was 1000 mL, and all experiments were performed at room temperature (27 °C).

Firstly, the open circuit potential (OCP) values of the samples were measured before performing the electrochemical corrosion tests. The OCP levels were measured for 2–3 h until a stable OCP was obtained, and then the OCP values were considered stable when the OCP curves had an asymptotically stable region. Then, Tafel measurements were carried out by polarizing the samples from −250 mV vs. OCP to +250 mV vs. OCP at a scanning rate of 1.0 mV/min.

3. Results and discussions

3.1. Characterization of the Loc/PEG-Ag NPs

In this study, a green Loc/PEG binary biopolymer blend was used as a stabilizing agent to obtain Ag NPs. The binary biopolymer matrix was used to control the particle size, particle dispersion, and stability of the structure. SEM and AI-aided SEM techniques were used to determine the particle size and distribution of Loc/PEG-Ag NPs. The surface characteristic results of (a) pure Loc, b) Loc/PEG-Ag NPs, and c) AI-aided SEM image of the Loc/PEG-Ag NPs were given in Fig. 2. According to the SEM results, we observed that Loc had a smooth surface (Fig. 2a). Loc/PEG-Ag NPs had a spherical shape with particle diameters smaller than 70 nm (Fig. 2b). However, according to the SEM images obtained, a clear surface property of the Loc/PEG-Ag NPs could not be observed. For this reason, we investigated the particle size of the nanostructure and the interaction between the Ag NPs and the matrix by providing their artificial intelligent (AI) supported SEM image data of the prepared Loc/PEG-Ag NPs. It was clear that the Loc/PEG-Ag NPs had a spherical shape and small particles in the size range of 30 to 70 nm (Fig. 2c). In the AI-aided SEM image of the Loc/PEG-Ag NPs, the biopolymer matrix and Ag were represented by green and red, respectively. The elemental composition and mapping diagram of the Loc/PEG-Ag NPs were characterized using the SEM/EDS technique. The SEM/EDS elemental mapping of the Loc/PEG-Ag NPs showed evidence of 48.1 % carbon (C), 34.8 % oxygen (O), 14.9 % silver (Ag), and 2.2 % sodium (Na) in the

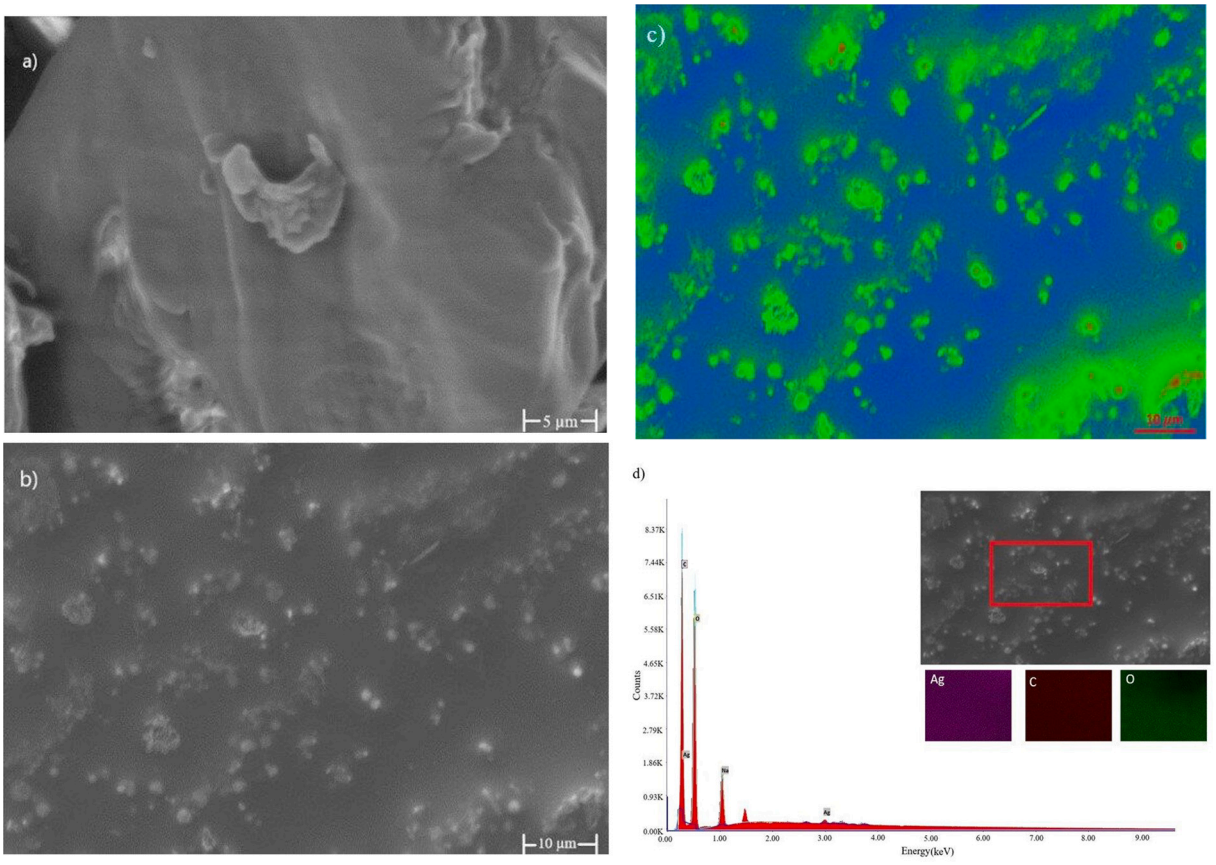

Fig. 2. SEM images of the a) pure Loc, b) Loc/PEG-Ag NPs, c) AI-aided SEM image of Loc/PEG-Ag NPs, and d) SEM/EDS.

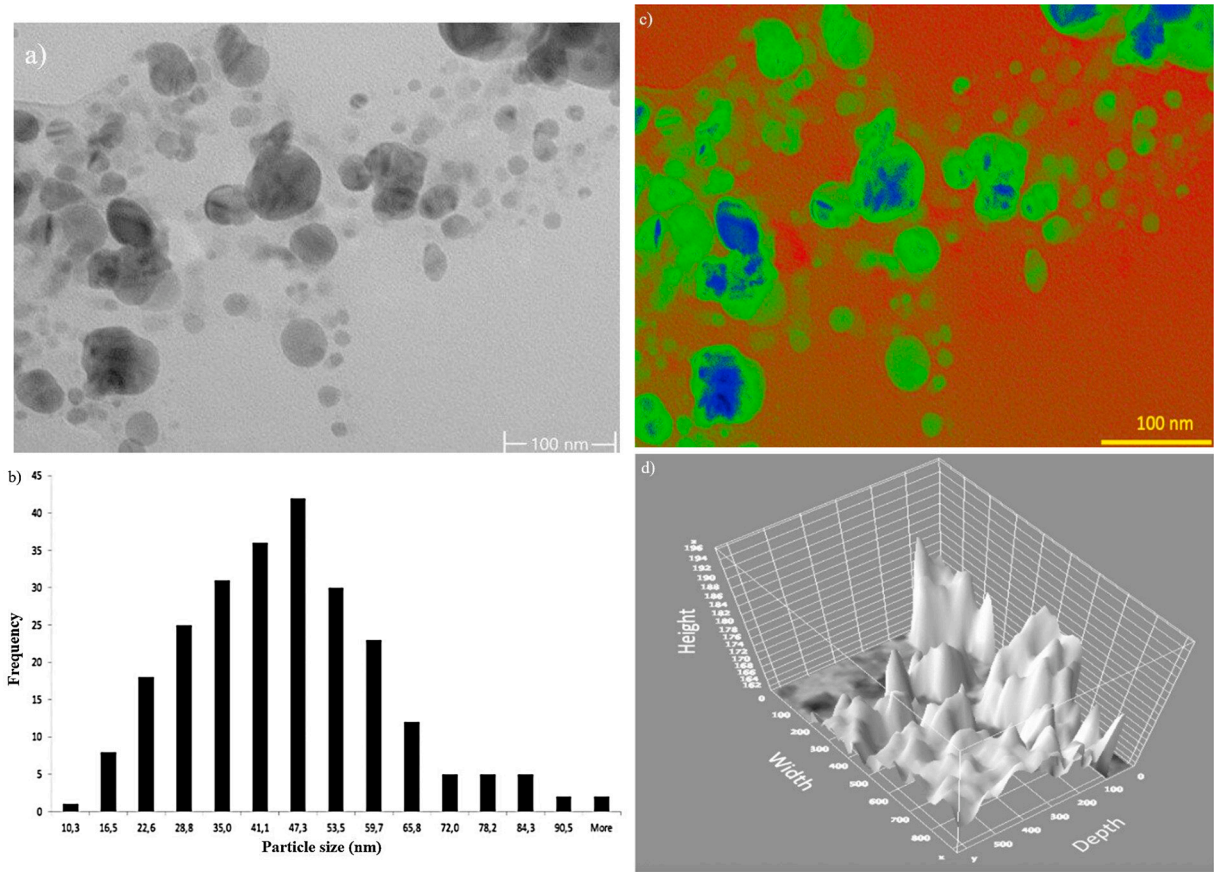

Fig. 3. a) TEM image of the Loc/PEG-Ag NPs, b) Particle size distribution histogram, c) AI aided TEM image of the Loc/PEG-Ag NPs, and d) 3D plot of the Loc/PEG-Ag NPs.

samples (Fig. 2d). The characteristic absorption peaks of the Loc/PEG-Ag NPs in the range of 1 and 3 keV were observed. Consequently, the shape, size, and distribution of the NPs are compatible with the studies in which Ag NPs were synthesized by the sonochemical method [53].

The surface property of Loc/PEG-Ag NPs was determined using the TEM technique. The morphology results of a) TEM image of the Loc/PEG-Ag NPs, b) particle size distribution histogram, c) AI-aided TEM image of the Loc/PEG-Ag NPs, and d) 3D plot of the Loc/PEG-Ag NPs were presented in Fig. 3. According to the TEM results, it was shown that Loc/PEG-Ag NPs had a spherical shape with particle diameters smaller than 50 nm (Fig. 3a). According to the particle size distribution histogram of the Loc/PEG-Ag NPs, the particle size was about 41.1 nm (Fig. 3b). In the AI-aided TEM image of the Loc/PEG-Ag NPs, the biopolymer matrix and Ag were represented by green and blue, respectively. Additionally, the AI-supported TEM image of the prepared Loc/PEG-Ag NPs showed that the Ag NPs had a spherical shape with NPs in the size range of 40 to 50 nm (Fig. 3c). According to the 3D surface analysis result of the Loc/PEG-Ag NPs, it was observed that the Ag NPs were homogeneously distributed with good dispersion in the Loc/PEG matrix (Fig. 3d). These TEM results were in agreement with the SEM results.

The XRD analysis of Loc/PEG-Ag NPs was performed to determine the crystal size of Ag NPs in the multifunctional nanobiocomposite structure. The XRD pattern graph of Loc/PEG-Ag NPs were given in Fig. 4a. As shown in Fig. 4a, the characteristic peaks of nanobiocomposite were formed $2\theta = 21.30°$, 38.60°, 44.40°, 65.60°, and 77.80°. The peaks of Loc/PEG-Ag NPs (38.60°, 44.40°, 65.60°, and 77.80°) correspond to planes of (111), (200), (220) and (311), respectively [49,54,55]. The characteristic peaks of the synthesized multifunctional Ag NPs corresponded to JCPDS file No.00–004–0783. Based on this, the silver crystal has a face-centered cubic structure [54,55]. Apart from the stated peaks, the peak observed at 21.30° was due to the bioorganic phase [9]. The average size of the crystal size of the Loc/PEG-Ag NPs was to be 17 nm using Eq. (2.1).

The FTIR analysis of (1) pure Loc powder and (2) Loc/PEG-Ag NPs was performed to determine the functional groups of samples in the wavenumber region between 4000 and 400 cm^{-1}. FTIR spectra of the samples were given in Fig. 4b. The characteristic FTIR peaks of the Loc were found at 3277 (-OH stretching), 2890 (C—H stretching), 1639 (-OH bending), 1376 (C—H bending), 1250 (C—O bending vibration), and 1012 (C-O-C stretching) cm^{-1}, respectively. The FTIR graph of Loc/PEG-Ag NPs exhibited absorption bands at 3393 (−OH stretching), 2871 (C—H stretching), 1649 (-OH bending), 1571 (-CH_3), 1457 (COO-), 1248 (C—O bending vibration), 1086 (C-O-C symmetrical stretching), and 945 (C-O-C symmetrical stretching) cm^{-1}, respectively. Consequently, it was confirmed by the FTIR graph at 518 cm^{-1} corresponding to the Ag (0) vibration present in the structure [56].

The UV–Vis measurement was performed to obtain the wavelength and absorbance spectrum of Ag NPs in the multifunctional nanobiocomposite structure. The UV–Vis results of Loc/PEG-Ag NPs were

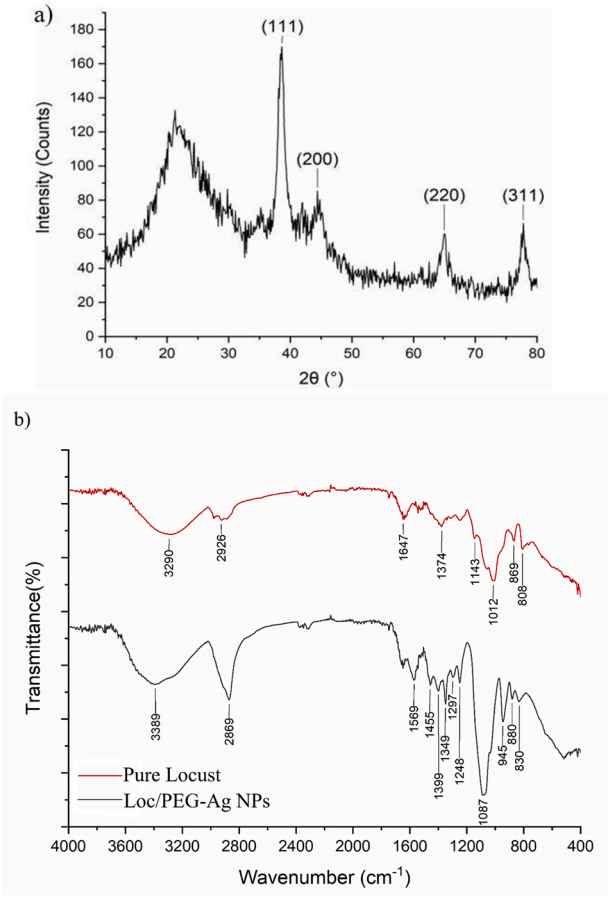

Fig. 4. a) XRD pattern of Loc/PEG-Ag NPs and b) FTIR spectra of pure Loc, and Loc/PEG-Ag NPs.

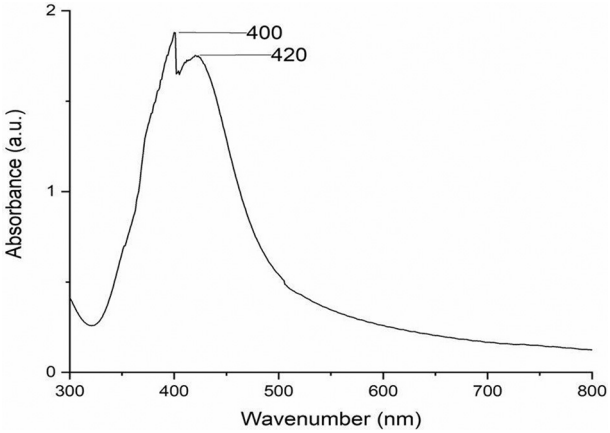

Fig. 5. UV–Vis spectra of Loc/PEG-Ag NPs.

given in Fig. 5. As seen in the spectrum, the formation of Ag NPs in the nanobiocomposite structure was indicated by the presence of the Ag^0 peak at 400–420 nm [57].

XPS analysis was carried out to investigate the surface properties, the elemental composition, and oxidation states of elements in the Loc/PEG-Ag NPs. The binding energies at 281.90 eV for C_{1s}, 530.00 eV for O_{1s}, and 365.10 eV for $Ag_{3d5/2}$ were assigned in Fig. 6a-d. The C_{1s} spectrum of the prepared Loc/PEG-Ag NPs was determined with two components at about 281.90 eV and 285.90 eV. All components at binding energies were observed at 281.90 eV and 285 eV (the nonoxygenated ring carbon (C—C), respectively (Fig. 6b). The O_{1s} spectrum (530.00 eV for O_{1s}) was observed for the prepared Loc/PEG-Ag NPs in Fig. 6c. In Fig. 6d, the signals at binding energies of 370.80 eV and 365.10 eV corresponded to the 3d3/2 and 3d5/2 orbits of metallic silver (Ag(0)) [58]. The splitting of the Ag_{3d} orbital doublet was 5.7 eV with respect to the formation of Ag(0).

The procedure for fabricating Loc/PEG-Ag NPs using fungal filtrate was based on the optimization strategy under constant temperature (25 °C), viscosity (2000 cP), and pH 7.4. According to our experimental results, the estimated sono-synthesis mechanism for the preparation of Loc/PEG-Ag NPs was given in Eqs. (3.1)–(3.4).

$$H_2O \rightarrow OH^* + H^* \quad (3.1)$$

$$OH^* + OH^* \rightarrow H_2O_2 \quad (3.2)$$

$$AgNO_3 \rightarrow Ag^+ + NO_3^- \quad (3.3)$$

$$Loc/PEG + Ag^+ + OH^- \rightarrow Loc/PEG - Ag\ NPs....OH \quad (3.4)$$

In brief, Loc/PEG mediated sono-synthesis can reduce Ag^+ to Ag^0 using functional groups such as O—H and = C-H in the organic polymer matrix under ultrasonic irradiation.

3.1.1. *Total antioxidant capacity of the Loc/PEG-Ag NPs*

The antioxidant capacity of a material is so important due to some reasons. Especially, by preventing radical chain reactions, antioxidants prevent the formation of very harmful free radicals (reactive oxygen and nitrogen species), which may cause a shortening of the shelf life of developed materials. Furthermore, antioxidants may ensure the oxidative stability of the nanocomposites [59–61]. Polyphenolics can exhibit their antioxidant activity (AO) in several ways: (i) Radical scavenging activity toward either reactive species (e.g., reactive oxygen species: ROS) such as ·OH, $O_2^{\bullet-}$, $^1O_2$, or toward lipid peroxidizing radicals such as R·, RO·, and ROO·; radical scavenging action generally proceeds via hydrogen atom transfer or electron donation; (ii) prevention of the transition metal-catalyzed production of reactive species (i.e., via Fenton type reactions) through metal chelation; (iii) interaction with other antioxidants (such as cooperative actions), localization, and mobility of the antioxidant at the microenvironment [62].

The spectrophotometric CUPRAC and ABTS/HRP assays were applied to evaluate the TAC of the Loc/PEG-Ag NPs sample. Results obtained are calculated as mmol TE g^{-1} where Trolox is used as the standard reference compound, as summarized in Table 3. According to these results, the values of TAC of Loc/PEG-Ag NPs are 17.90 ± 0.50 mmol TE g^{-1} and 20.47 ± 0.19 mmol TE g^{-1} for CUPRAC and ABTS/HRP assays, respectively. As can be seen in Table 3, the TAC values obtained by both methods are quite compatible. Furthermore, the proposed nanobiocomposite has high antioxidant capacity.

In the present study, the CUPRAC method was applied for the first time for determining the TAC of Loc/PEG-Ag NPs in the literature. In the study of Mumtaz Hamdani and Ahmed Wani, the ABTS assay was used to measure the radical scavenging activities of the methanolic and ethanolic guar and Loc extracts. The antioxidant activity of Loc was found to be 0.63 and 0.40 μM ascorbic acid equivalents in mg/100 g (μM AAE in mg/100 g) of the sample for methanolic and ethanolic extracts, respectively [59]. In another study, the antioxidant capacity of carob seed was measured as 15.71 and 14.01 mM TE g^{-1} dry weight by using the CUPRAC and ABTS assays, respectively [60]. Castro-Lopez et al.

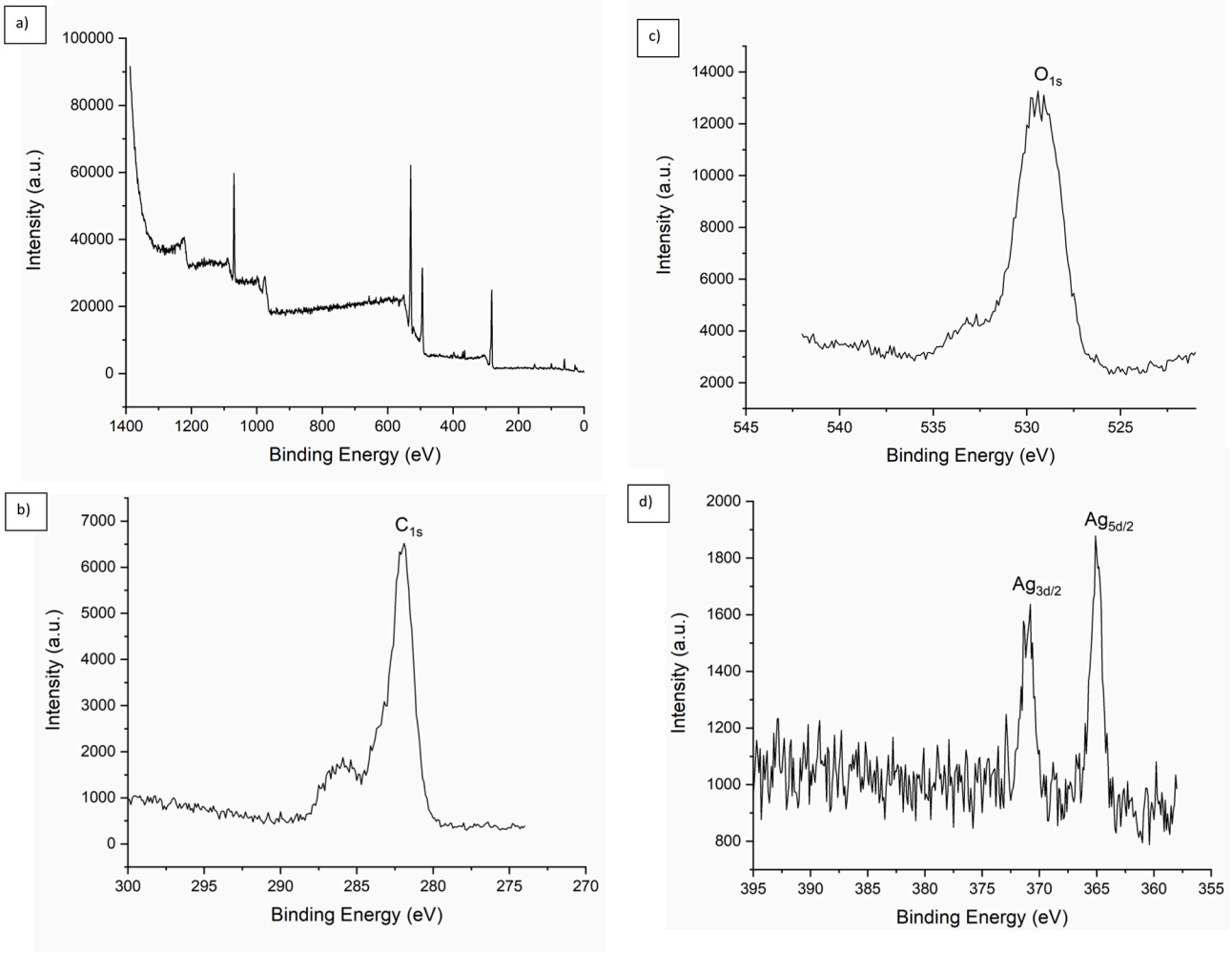

Fig. 6. XPS spectra of Loc/PEG-Ag NPs: a) XPS survey spectrum b) binding energy spectrum for C_{1s} c) binding energy spectrum for $O_{1s,}$ and d) binding energy spectrum for Ag_{3d}.

Table 3
The TAC of Loc/PEG-Ag NPs in the units of mmol TE g^{-1} concerning the CUPRAC and ABTS/HRP assays ($n = 3$).

Sample	CUPRAC	ABTS/HRP
Loc/PEG-Ag NPs	17.90 ± 0.50[a]	20.47 ± 0.19[a]

[a] Total antioxidant capacities of the Loc/PEG-Ag NPs were expressed as mol TR g^{-1}.

extracted and encapsulated *Moringa oleifera* leaves and investigated the influence of Loc by using different methods [61]. According to the ABTS method, the antioxidant capacity of Loc alone was found to be 6.14 mg TE g^{-1} where it was determined to be 5169 mg TE g^{-1} in terms of the ABTS/HRP method in the same unit for Loc/PEG-Ag NPs nano-biocomposite as 842 times higher.

3.2. Characterization of the Loc/PEG-Ag NPs coated SS316L

3.2.1. Superficial and microstructural characterizations

SEM images of the coated samples with drop casting and airbrush spray methods are given in Figs. 7 and 8, respectively. In both coating methods, it is seen that the surfaces are successfully coated. It is important to examine both methods to improve the homogeneity of the coated areas and increase the density of the NPs on the SS316L. When the surface morphologies of both coating methods are examined, it is seen that the coating is rough, defect-free, crack-free, and monolayered. In both techniques, the adhesion between the coating and the substrate is not very strong. The reason for this situation, Soloviev and Gedanken explained that the NPs do not adhere to the surface unless they move rapidly [63]. NPs passing through the fluid slow down due to friction and accumulate on the stainless steel surface, especially with airbrush spray techniques. The effects on the surface morphologies of the coating with the airbrush spray methods are that: (i) leads to more agglomeration on the surface; (ii) the particle structure accumulated on the surface is clearer; and (iii) NPs are not fully embedded in the surface. Velasco et al. stated that the mobility of Ag NPs was unrestricted and continued in its direction to move over the coated surface as agglomerated Ag NPs at a nearly complete deposition process [64].

SEM images of the coated surface clearly showed the difference

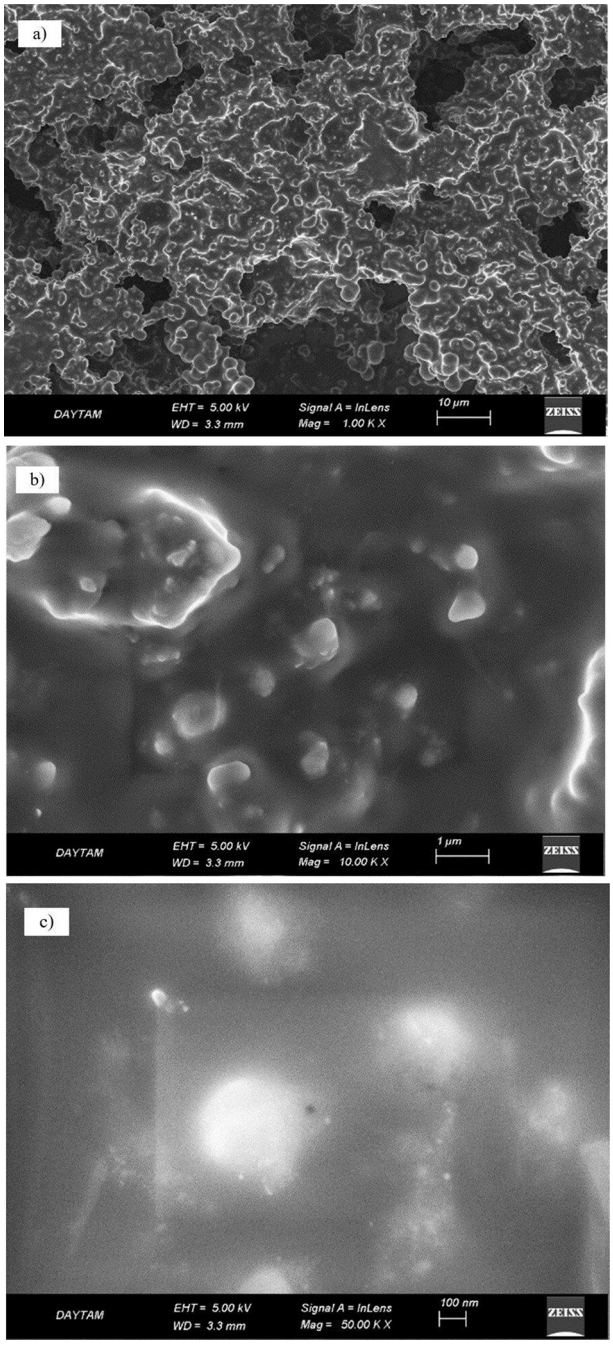

Fig. 7. SEM images of the drop casting coated sample at different magnifications a) x100, b) x10000, and c) x50000.

between coating techniques. Due to their rough surface formation, their surface tension is low, and correspondingly, these surfaces are considered to have high hydrophobic properties. These features are more dominant on airbrush spray coated surfaces than on drop casting coated surfaces. In both coatings, the multifunctional NPs were uniformly distributed throughout the coating layer, but this uniformity was more pronounced in the airbrush spray coating. The homogeneous distribution and coating of Ag NPs improve the resistivity properties of the substrate. Jothi et al. coated with Ag NPs on SS304 and stated that the resistance properties of the substrate increased with the homogeneous distribution of the NPs [33]. The structure of the coating obtained with

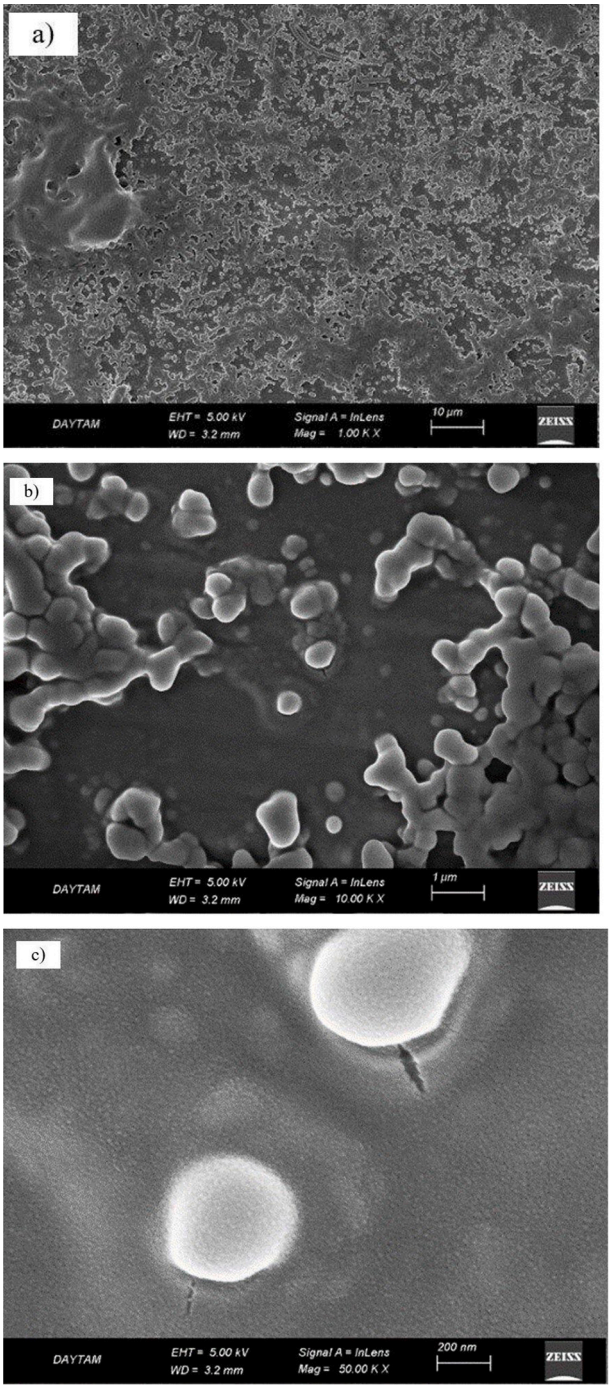

Fig. 8. SEM images of the airbrush spray coated sample at different magnifications a) x100, b) x10000, and c) x50000.

Table 4
Average surface roughness results of the uncoated and coated samples.

Sample	Average Roughness (Ra, µm)
Uncoated SS316L	1.281
Drop casting sample	1.023
Airbrush coated sample	1.120

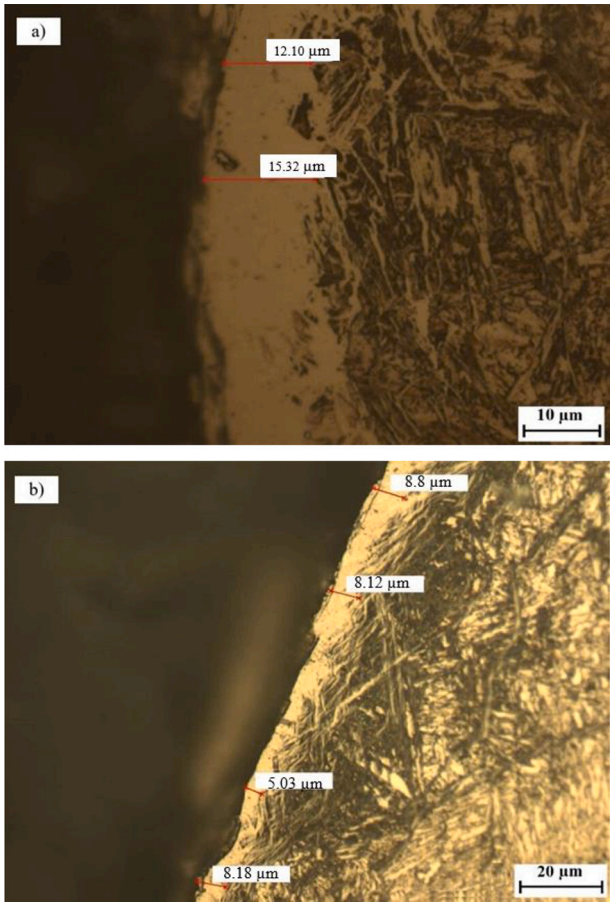

Fig. 9. Cross-sectional view of coated samples a) drop cast and b) airbrush spray.

propanoic leaf extracts of Ag NPs is similar to the morphology in this study, especially with the drop casting coated structure.

In Table 4, the average surface roughness (Ra) values are given for the uncoated SS316L part and the coated samples by drop casting and airbrush spray methods for comparison. Uncoated, drop cast, and airbrush spray coated samples had Ra values of approximately 1.281 µm, 1.023 µm, and 1.120 µm, respectively. In the surface roughness measurements, it was observed that the surface roughness value of the surfaces coated with both methods was lower than the uncoated SS316L. It can be said that this is due to the measurement being micron-level and the coated particles being nanoscale. However, when the comparison between the two coating methods was made, it was determined that the surface roughness value was higher in the SS316L coated with the airbrush spray coating method. High surface roughness is a desirable feature for metallic biomedical surfaces. Because high surface roughness allows cells to adhere, spread, and grow while preventing the adhesion of bacteria [65–67]. For some biomaterials, the fine and medium surface roughness values vary between 0.5–1 µm and 1–2 µm, respectively [68]. In this case, the values obtained in the coating techniques have a medium surface roughness value and are promising for use in biomedical applications. According to Jothi et al., the surface roughness properties of the coating affect many properties, such as its hydrophobic character, interaction with bacteria and abrasives [33]. These properties are enhanced by increased surface roughness. According to this approach, the roughness values obtained in our study are also significant.

In Fig. 9, the cross-sectional view of the drop casting and airbrush spray coatings made on the SS316L surface with Ag NPs were given. In all samples, a uniform transition interface was formed between the substrate and the Ag NPs coating. The interface coating thickness values of Loc/PEG-Ag NPs coated on SS316L by drop casting and airbrush spray were measured using an optical microscope in the range of 12–15 µm and 6–8 µm, respectively. According to optical microscope images, two coating processes applied to the SS316L were effective. It is seen that the coatings exhibit continuity in the side section surface morphology examinations. There is no crack or delamination formation throughout the interface.

The 3-Dimensional (3D) surface images of the coatings made by the drop casting method and the airbrush spray methods were given in Fig. 10a and b, respectively. In the images of the examined areas, it is seen that the coating thickness is 15.03 µm in the drop casting coated sample, while an 8.47 µm coating was obtained in the airbrush spray coated sample. The coating of Ag NPs as a homogeneous and single-layered structure on the stainless steel surface was carried out. This coating structure is defined as a monolayer structure in the literature [13].

The distribution of Loc/PEG-Ag NPs the colony particles in the Z direction was unsymmetrical for samples coated with both techniques, especially the airbrush spray technique. The main reason for this is thought to be that the coating with the airbrush spray technique is faster and does not allow NPs to be embedded in the surface. According to Wojcieszak [69], the surface had a minimal value in the Z direction and the low intensity of Ag NPs is due to the speed of the coating. Roldan et al. correlated scattering with surface roughness and discovered that scattering increases as surface roughness increases [70]. This explanation also supports our results.

3.2.2. *Antibacterial activity*

Although SS316L is widely used in various medical applications, it

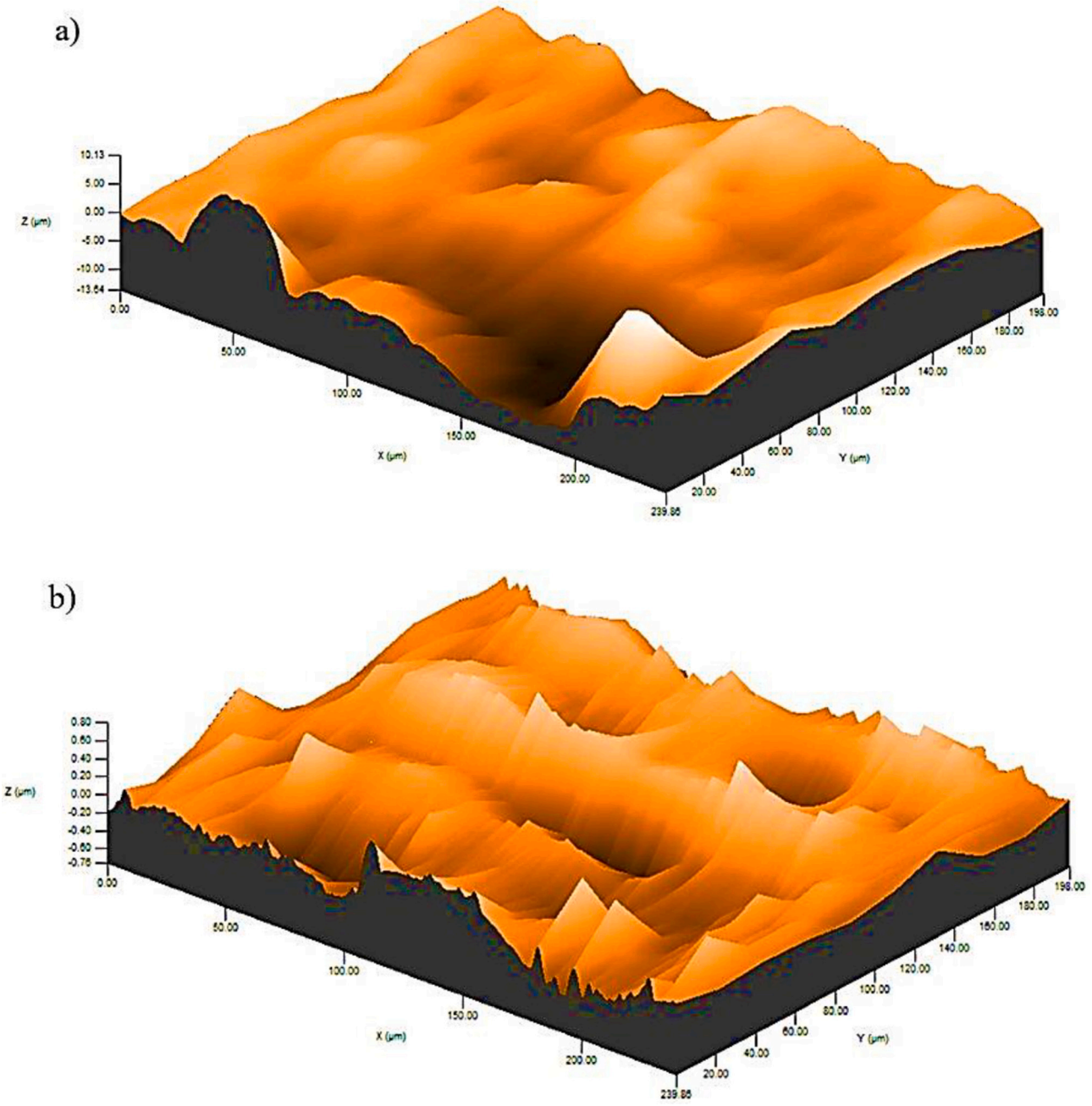

Fig. 10. 3D surface profile of a) drop cast and b) airbrush spray coated samples.

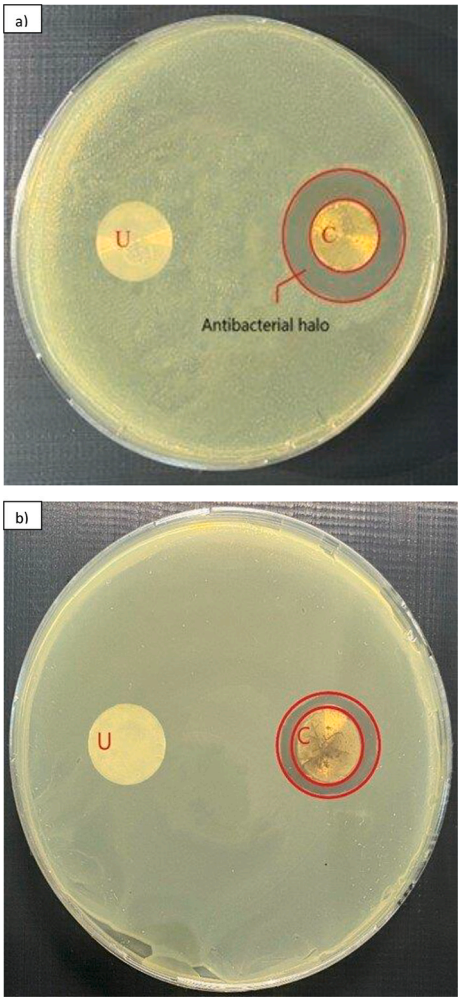

Fig. 11. Antibacterial activity against a) *E. coli* b) *S. aureus* (U: Uncoated, C: Coated).

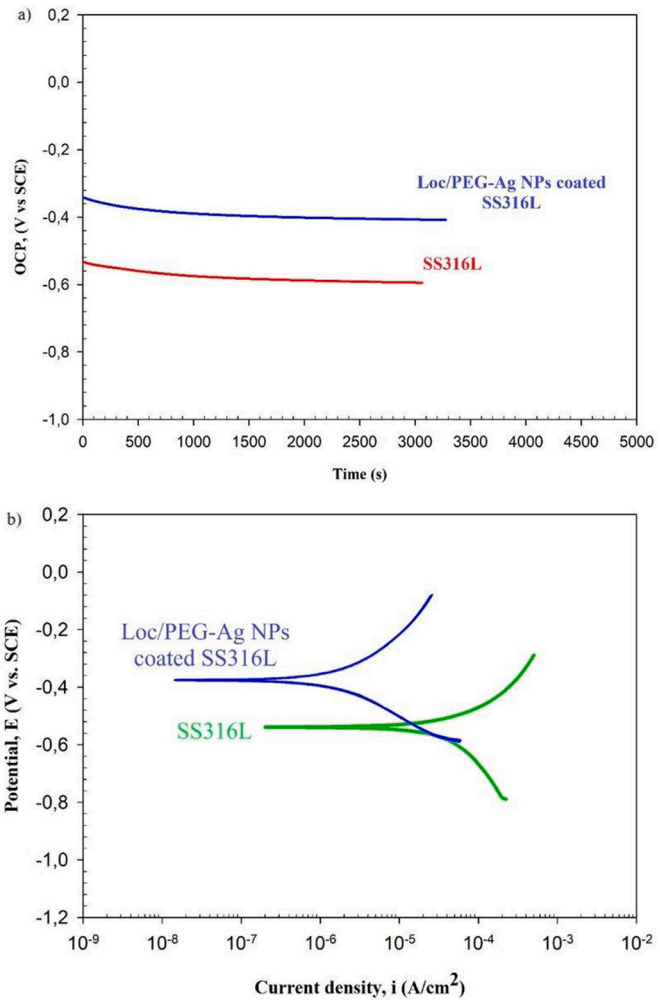

Fig. 12. a) OCP and b) potentiodynamic polarization curves of Loc/PEG-Ag NPs coated SS316L and uncoated SS316L.

lacks antibacterial properties due to the easy growth of bacterial colonies on the surface of SS316L [71]. Therefore, it is necessary to enhance the antibacterial properties of SS316L. One of the most effective ways to achieve this purpose is to deposit a protective Ag NPs coating on the surface of 316L. For this purpose, the SS316 L were coated with the synthesized Loc/PEG-Ag NPs in this study. The prepared Loc/PEG-Ag NPs coated SS316 L was tested for antibacterial activity against the gram-negative (*E. coli*) and gram-positive (*S. aureus*) pathogens by following the agar well diffusion method. As seen in Fig. 11, the prepared Loc/PEG-Ag NPs exhibited antibacterial activity against all bacterial strains. The ZOI was recorded after 24 h of incubation time at 37 °C. The coated surfaces with Loc/PEG-Ag NPs showed an antibacterial activity which was proven by the appearance of ZOI against *E. coli* (Fig. 11a) and *S. aureus* (Fig. 11b) pathogens at 28 mm and 19 mm, respectively. The role of the Loc/PEG-Ag NPs coating in resistance for these bacteria was higher for *E. coli*, as shown in Fig. 11a. The control groups (uncoated samples), on the other hand, exhibited no antibacterial activity against pathogens. Considering the metal-based nanosystems with biological performance, it was indicated that the sono-synthesized Ag NPs are promising antibacterial coating materials. It has been emphasized in the literature that smaller Ag NPs with large surface area have a better bactericidal effect compared to larger particles [49]. In this study, we assumed that the possible antibacterial mechanism of the Loc/PEG-Ag NPs is based on the small particle size and interaction based on the large surface area. It has been discussed in many scientific studies that silver ions have a high antibacterial effect against *E. coli* and *S. aureus* [72,73]. Thus, our results are in agreement with the studies previously reported in the literature. Understanding the antibacterial mechanism will primarily enable the use of Loc/PEG-Ag NPs as a potent large-scale antibacterial agent for their wide applications in various fields.

3.2.3. *Electrochemical corrosion test*

On the other hand, SS316L can be easily corroded when in contact with the body fluids. To avoid this situation, it is very important to understand and improve the corrosion resistance of the SS316L surface. For this purpose, the corrosion behavior of airbrush spray coated and uncoated surfaces was investigated. The OCP curves were drawn to examine the electrochemical corrosion performance of coated and uncoated SS316L. Fig. 12a shows the effects of the Loc/PEG-Ag NPs coating on the OCP curves obtained in the Ringer's solution. The fact that any material has a high OCP value in an environment means that the material is more stable in that environment [74]. In the uncoated sample, the potential stood at a stable of −0,61 *V*, whereas in the Loc/PEG-Ag NPs coated sample, it exhibited a nobler potential value of −0.39 V. In comparison, the OCP value of the Loc/PEG-Ag NPs coated sample remained at a relatively stable level during the whole test time. It is seen that the Loc/PEG-Ag NPs coated sample is more stable in the Ringer's solution environment than the uncoated sample. Tafel curves were used to investigate the corrosion behavior. As seen in Fig. 12b, the uncoated SS316L sample has lower resistance to electrochemical corrosion and higher corrosion current density (I_{corr}). The value of I_{corr}

Table 5
Techniques for the preparation, antibacterial, and corrosion properties of Ag NPs coated on various metallic materials.

Substrate	Coating	Coating Technique	Antibacterial Activity			Corrosion Behavior	Reference
			Pathogen	Assay	Activity		
SS316L	Ag NPs/ PTFE	Sol-gel dip coating	*E. coli*	–	90 % (for 24 h)	Potentiodynamic polarization in PBS	[10]
SS316L	Ag NPs/ Gelatin	Airbrush spray coating	*S. aureus*	Disk diffusion	10–20 mm	Not tested	[49]
2507 duplex SS	HAp/Ag NPs	Electrophoretic deposition	*E. coli*	Inhibition of bacterial growth	Active vs. each bacterial strains	Anticorrosive behavior in Ringer's solution	[35]
			S. aureus				
Titanium sheet	PEGDA-AA hydrogel/ Ag NPs	Electropolymeri-zation & dip coating	*E. coli*	Inhibition of bacterial growth	Active vs. each bacterial strains	Not tested	[12]
			S. aureus				
SS316L	PDA-Ag NPs	Dip coating	*E. coli*	Inhibition of bacterial growth	A smaller amount of cells adhered to *E.coli* than *S. aureus* (24 h)	Corrosive behavior in 3.5 wt% NaCl solution	[48]
			S. aureus				
SS304	SiO_2@ P.niruri- Ag NPs	Sol-gel dip coating	*E. coli*	Inhibition zone	5–16 mm	Anticorrosive behavior for 1 h in a 3.5 wt% NaCl solution	[33]
SS316L	Loc/PEG-Ag NPs	Airbrush spray coating	*E. coli*	Disk diffusion	28 mm for *E.coli*	Anticorrosive behavior in Ringer's Solution	This study
			S. aureus		19 mm for *S. aureus*		

was decreased after coating with Loc/PEG-Ag NPs. The coated sample has higher corrosion resistance than the uncoated sample. Results indicate that the Loc/PEG-Ag NPs coating successfully obtained a novel protective film on the surface of SS316L, and with this coating, the occurrence of electrochemical corrosion is prevented. It is seen in the literature that coatings with Ag NPs increase the corrosion resistance of the metal substrate. The results are consistent with the previous studies in the literature [10,35].

A summary of the scientific studies dealing with the antibacterial effect and corrosion performance of the Ag NPs deposited on the surface of the different metallic substrates were reported in Table 5. One of the most important solutions related to the industrial development of innovative multifunctional coatings is the development of surfaces with NMs. In this regard, coating techniques and materials come to the fore. The coating technique used in this study has many advantages over the other techniques that were given in the table. These are; (i) It is possible to use different materials that can be coated on the surfaces such as metal and metal oxides; (ii) It requires simple equipment and inexpensive consumables; (iii) It is possible to coat the parts with complex shapes and different sizes. The experimental results showed that the fabrication of multifunctional antioxidant, antibacterial, and anticorrosive Loc/PEG-Ag NPs has great potential in biomedical coating applications. It is known that nanostructured coated steel is also a promising material for several biomedical and pharmaceutical applications. With the unique biological performance of nanostructure-based surfaces, this study provided a green Loc/PEG-Ag NPs-based strategy for surface coatings.

4. Conclusions

In this study, novel multifunctional Ag NPs in the organic biomatrix (Loc/PEG) was successfully synthesized using a green sonochemical method. The Ag NPs were coated on the SS316L surface with two different coating techniques such as drop casting and airbrush spray. The Loc/PEG-Ag NPs deposited on SS316L were analyzed to determine the morphological characteristics, superficial properties, antibacterial activity, and corrosion resistivity. Based on the results, we reached the following conclusions:

- Ag NPs were homogeneously distributed with good dispersion in the Loc/PEG matrix. The synthesized Loc/PEG-Ag NPs have an average size distribution of 41.1 nm and a spherical shape.
- The TAC of the Loc/PEG-Ag NPs values of the nanobiocomposite are quite high.
- The surface modification of SS316L enriched with more homogeneously dispersed Ag NPs is improved, especially for airbrush spray coated substrates.
- The Ra values obtained in both coating methods are medium in classification and so suitable for use in metallic biomaterials.
- In the examination of the cross-sectional surface morphologies of the both coatings, no cracks and delamination formation were observed along the interface.
- According to the surface profile measurement results, the morphology of the coatings was uniform and homogeneous for both coatings.
- The coating methods used in this study are a simple, low-cost, and fast way of deposition, especially for smaller substrates. The airbrush spray coating method is promising for surface coating due to its applicability to complicated shaped surfaces, offering homogeneous distribution, and optimization of the process parameters.
- Ag NPs coated on SS316L play a key role in the development of antibacterial and anticorrosive properties. This study is of particular interest for the bio-functionalization of SS316L for its multifunctional surface properties.
- In conclusion, most of our hypotheses on improving the surface modification of SS316L are supported by the results of this study. Our

future work vision includes applications on different substrate materials with different coating techniques of Ag NPs deposited on SS316L as discussed in this study.
- This article can help researchers develop new procedures, methods and materials to achieve a modern scheme for the design of nano-modified antibacterial materials that are long-lasting, safe, and effective on corrosion and have broad bacterial infection properties.

CRediT authorship contribution statement

Gizem Karabulut: Data Curation, Writing-original draft, Validation, Methodology, Formal analysis. **Nuray Beköz Üllen:** Writing-Reviewing, Methodology, Supervision, and Resources. **Esin Akyüz:** Formal analysis. **Selcan Karakuş:** Writing-Reviewing, Methodology, Validation, and Resources.

Declaration of competing interest

The authors declare the following financial interests/personal relationships which may be considered as potential competing interests: Gizem KARABULUT reports financial support was provided by Scientific Research Projects Coordination Unit of Istanbul University-Cerrahpasa.

Data availability

Data will be made available on request.

Acknowledgments

This study was funded by Scientific Research Projects Coordination Unit of Istanbul University-Cerrahpasa. Project number: FYL-2021-36085. The authors would like to thank Res. Asst. Ceyhun TORUNTAY of Istanbul Technical University for the assistance during the antibacterial tests.

References

[1] M. Chethipuzha, A.R. Abraham, N. Kalarikkal, S. Thomas, S. Sreeja, Embracing nanotechnology concepts in the electronics industry, in: Fundam. Prop. Multifunct. Nanomater, 2021, pp. 405–421, https://doi.org/10.1016/B978-0-12-822352-9.00004-3.
[2] M. Akbar Shah, B. Masood Pirzada, G. Price, A.L. Shibiru, A. Qurashi, Applications of nanotechnology in smart textile industry: a critical review, J. Adv. Res. 38 (2022) 55–75, https://doi.org/10.1016/J.JARE.2022.01.008.
[3] S.H. Khan, S.A. Alaie, Green nanomaterials for environmental applications, in: Green Nanomater.Ind. Appl, 2022, pp. 365–396, https://doi.org/10.1016/B978-0-12-823296-5.00012-5.
[4] A. Rajput, R. Keshari, R. Patil, R. Banerjee, Nanobiomaterials for wound healing, Nanotechnol. Med. Biol. (2022) 109–139, https://doi.org/10.1016/B978-0-12-819469-0.00004-6.
[5] L.H. Madkour, Applications of nanomaterials and nanoparticles, Adv. Struct. Mater. 116 (2019) 565–603, https://doi.org/10.1007/978-3-030-21621-4_15.
[6] P.G. Jamkhande, N.W. Ghule, A.H. Bamer, M.G. Kalaskar, Metal nanoparticles synthesis: an overview on methods of preparation, advantages and disadvantages, and applications, J. Drug Deliv. Sci. Technol. 53 (2019), 101174, https://doi.org/10.1016/j.jddst.2019.101174.
[7] Shahid-ul-Islam, B.S. Butola, A. Kumar, Green chemistry based in-situ synthesis of silver nanoparticles for multifunctional finishing of chitosan polysaccharide modified cellulosic textile substrate, Int. J. Biol. Macromol. 152 (2020) 1135–1145, https://doi.org/10.1016/J.IJBIOMAC.2019.10.202.
[8] V.P. Veeraraghavan, N.D. Periadurai, T. Karunakaran, S. Hussain, K.M. Surapaneni, X. Jiao, Green synthesis of silver nanoparticles from aqueous extract of Scutellaria barbata and coating on the cotton fabric for antimicrobial applications and wound healing activity in fibroblast cells (L929), SaudiJ. Biol. Sci. 28 (2021) 3633–3640, https://doi.org/10.1016/J.SJBS.2021.05.007.
[9] F. LewisOscar, C. Nithya, S. Vismaya, M. Arunkumar, A. Pugazhendhi, P. Nguyen-Tri, S.A. Alharbi, N.S. Alharbi, N. Thajuddin, In vitro analysis of green fabricated silver nanoparticles (AgNPs) against Pseudomonas aeruginosa PA14 biofilm formation, their application on urinary catheter, Prog. Org. Coat. 151 (2021), 106058, https://doi.org/10.1016/J.PORGCOAT.2020.106058.
[10] S. Zhang, X. Liang, G.M. Gadd, Q. Zhao, A sol–gel based silver nanoparticle/polytetrafluorethylene (AgNP/PTFE) coating with enhanced antibacterial and anti-corrosive properties, Appl. Surf. Sci. 535 (2021), 147675, https://doi.org/10.1016/J.APSUSC.2020.147675.
[11] Y. Cai, X. Luo, M. Maclean, Y. Qin, M. Duxbury, F. Ding, A single-step fabrication approach for development of antimicrobial surfaces, J. Mater. Process. Technol. 271 (2019) 249–260, https://doi.org/10.1016/J.JMATPROTEC.2019.04.012.
[12] E. De Giglio, D. Cafagna, S. Cometa, A. Allegretta, A. Pedico, L.C. Giannossa, L. Sabbatini, M. Mattioli-Belmonte, R. Iatta, An innovative, easily fabricated, silver nanoparticle-based titanium implant coating: development and analytical characterization, Anal. Bioanal. Chem. 405 (2013) 805–816, https://doi.org/10.1007/s00216-012-6293-z.
[13] R. Alias, R. Mahmoodian, M.H. Abd Shukor, Development and characterization of a multilayer silver/silver-tantalum oxide thin film coating on stainless steel for biomedical applications, Int. J. Adhes. Adhes. 92 (2019) 89–98, https://doi.org/10.1016/J.IJADHADH.2019.04.010.
[14] F. Bir, H. Khireddine, Z. Mekhalif, S. Bonnamy, Pulsed electrodeposition of Ag+ doped prosthetic Fluorohydroxyapatite coatings on stainless steel substrates, Mater. Sci. Eng. C 118 (2021), 111325, https://doi.org/10.1016/J.MSEC.2020.111325.
[15] S.H. Bindu, S.V.K. Vani, G. Nirisha, N. Madhuri, B.S. Deepa, S. Hemadri, Evaluation of antibacterial effect of silver nanoparticle coated stainless steel band material – an in vitro study, Orthod. J. Nepal 9 (2019) 13–19, https://doi.org/10.3126/OJN.V9I2.28404.
[16] S.A. Gawad, A. Nasr, A.M. Fekry, L.O. Filippov, Electrochemical and hydrogen evolution behaviour of a novel nano-cobalt/nano-chitosan composite coating on a surgical 316L stainless steel alloy as an implant, Int. J. Hydrog. Energy 46 (2021) 18233–18241, https://doi.org/10.1016/J.IJHYDENE.2021.03.018.
[17] D. Xu, S. Guo, G. Jiang, Y. Li, J. Yang, W. Kuang, Superior protective performance of NiCr coating on stainless steel 316L in pure, oxygenated and chlorinated supercritical water, Surf. Coat. Technol. 432 (2022), 128029, https://doi.org/10.1016/J.SURFCOAT.2021.128029.
[18] M. Nadimi, C. Dehghanian, Incorporation of ZnO–ZrO2 nanoparticles into TiO2 coatings obtained by PEO on Ti–6Al–4V substrate and evaluation of its corrosion behavior, microstructural and antibacterial effects exposed to SBF solution, Ceram. Int. 47 (2021) 33413–33425, https://doi.org/10.1016/J.CERAMINT.2021.08.248.
[19] S. Velumani, G. Regmi, M. Lee, H. Castaneda, M. Kuttolamadom, X. Qian, A. Kassiba, Engineered Zr/Zn/Ti oxide nanocomposite coatings for multifunctionality, Appl. Surf. Sci. 563 (2021), 150353, https://doi.org/10.1016/J.APSUSC.2021.150353.
[20] M. Mathina, E. Shinyjoy, S. Ramya, L. Kavitha, D. Gopi, Multifunctional crab shell derived hydroxyapatite/metal oxide/polyhydroxybutyrate composite coating on 316L SS for biomedical applications, Mater. Lett. 313 (2022), 131701, https://doi.org/10.1016/J.MATLET.2022.131701.
[21] K. Xue, L.X. Liang, S.C. Cheng, H.P. Liu, L.Y. Cui, R.C. Zeng, S.Q. Li, Z.L. Wang, Corrosion resistance, antibacterial activity and drug release of ciprofloxacin-loaded micro-arc oxidation/silane coating on magnesium alloy AZ31, Prog. Org. Coat. 158 (2021), 106357, https://doi.org/10.1016/J.PORGCOAT.2021.106357.
[22] R. Ahmadi, N. Asadpourchallou, B.K. Kaleji, In vitro study: evaluation of mechanical behavior, corrosion resistance, antibacterial properties and biocompatibility of HAp/TiO2/Ag coating on Ti6Al4V/TiO2 substrate, Surf. Interfaces 24 (2021), 101072, https://doi.org/10.1016/J.SURFIN.2021.101072.
[23] S.T. Chen, H.W. Chien, C.Y. Cheng, H.M. Huang, T.Y. Song, Y.C. Chen, C.H. Wu, Y. H. Hsueh, Y.H. Wang, S.F. Ou, Drug-release dynamics and antibacterial activities of chitosan/cefazolin coatings on Ti implants, Prog. Org. Coat. 159 (2021), 106385, https://doi.org/10.1016/J.PORGCOAT.2021.106385.
[24] L. Li, Y. Wang, K. Liu, L. Yang, B. Zhang, Q. Luo, R. Luo, Y. Wang, Nanoparticles-stacked superhydrophilic coating supported synergistic antimicrobial ability for enhanced wound healing, Mater. Sci. Eng. C 132 (2022), 112535, https://doi.org/10.1016/J.MSEC.2021.112535.
[25] A. Santos-Coquillat, E. Martínez-Campos, H. Mora Sánchez, L. Moreno, R. Arrabal, M. Mohedano, A. Gallardo, J. Rodríguez-Hernández, E. Matykina, Hybrid functionalized coatings on metallic biomaterials for tissue engineering, Surf. Coat. Technol. 422 (2021), 127508, https://doi.org/10.1016/J.SURFCOAT.2021.127508.
[26] M. Zhu, X. Li, L. Ge, Y. Zi, M. Qi, Y. Li, D. Li, C. Mu, Green synthesis of κ-carrageenan@Ag submicron-particles with high aqueous stability, robust antibacterial activity and low cytotoxicity, Mater. Sci. Eng. C 106 (2020), 110185, https://doi.org/10.1016/J.MSEC.2019.110185.
[27] L. Gao, L. Wang, L. Yang, Y. Zhao, N. Shi, C. An, Y. Sun, J. Xie, H. Wang, Y. Song, Y. Ren, Preparation, characterization and antibacterial activity of silver nanoparticle/graphene oxide/diatomite composite, Appl. Surf. Sci. 484 (2019) 628–636, https://doi.org/10.1016/J.APSUSC.2019.04.153.
[28] C. Zhang, J. Huang, X. Lan, H. Qi, D. Fan, L. Zhang, Synergy of bioinspired chimeric protein and silver nanoparticles for fabricating "kill-release" antibacterial coating, Appl. Surf. Sci. 557 (2021), 149799, https://doi.org/10.1016/J.APSUSC.2021.149799.
[29] L. Hernández-Morales, H. Espinoza-Gómez, L.Z. Flores-López, E.L. Sotelo-Barrera, A. Núñez-Rivera, R.D. Cadena-Nava, G. Alonso-Núñez, K.A. Espinoza, Study of the green synthesis of silver nanoparticles using a natural extract of dark or white Salvia hispanica L. seeds and their antibacterial application, Appl. Surf. Sci. 489 (2019) 952–961, https://doi.org/10.1016/J.APSUSC.2019.06.031.
[30] M.A. Khan, W. Hussain, N. Hassan, M. IIyas, S.Z. Zill-e-huma, L.Hui Abbas, Fabrication of Ag nanoparticles on a Cu-substrate with excellent superhydrophobicity, anti-corrosion, and photocatalytic activity, Alex.Eng. J. 61 (2021) 6507–6521, https://doi.org/10.1016/J.AEJ.2021.12.010.
[31] A. Sultan, F. Mohammad, Chemical sensing, thermal stability, electrochemistry and electrical conductivity of silver nanoparticles decorated and polypyrrole enwrapped boron nitride nanocomposite, Polymer 113 (2017) 221–232, https://doi.org/10.1016/J.POLYMER.2017.02.074 (Guildf).

[32] A. Javadi, A. Solouk, M. Haghbin Nazarpak, F. Bagheri, Surface engineering of titanium-based implants using electrospraying and dip coating methods, Mater. Sci. Eng. C 99 (2019) 620–630, https://doi.org/10.1016/J.MSEC.2019.01.027.
[33] K. Jeeva Jothi, S. Balachandran, K. Palanivelu, Synergistic combination of Phyllanthus niruri/silver nanoparticles for anticorrosive application, Mater. Chem. Phys. 279 (2022), 125794, https://doi.org/10.1016/J.MATCHEMPHYS.2022.125794.
[34] A. Allion-Maurer, C. Saulou-Bérion, R. Briandet, S. Zanna, N. Lebleu, P. Marcus, P. Raynaud, B. Despax, M. Mercier-Bonin, Plasma-deposited nanocomposite polymer-silver coating against Escherichia coli and Staphylococcus aureus: antibacterial properties and ageing, Surf. Coat.Technol. 281 (2015) 1–10, https://doi.org/10.1016/J.SURFCOAT.2015.09.025.
[35] F.W. Abdulsada, A.S. Hammood, Characterization of corrosion and antibacterial resistance of hydroxyapatite/silver nano particles powder on 2507 duplex stainless steel, Mater. Today Proc. 42 (2021) 2301–2307, https://doi.org/10.1016/J.MATPR.2020.12.319.
[36] L. Hiremath, S. Nipun, O. Sruti, N.G. Kala, B.M. Aishwarya, Sonochemistry: applications in biotechnology, Sonochem.React. (2020) 1–11, https://doi.org/10.5772/INTECHOPEN.88973.
[37] S. Karakus, E. Tan, M. Ilgar, I.M. Kahyaoglu, Y.M. Şahin, D.S. Mansuroglu, D. Ismik, N. Tasaltin, A. Kilislioglu, Preparation, characterization, and swelling behavior of PEGylated guar gum @ Ag nanoparticles, Sonochem. React. (2019) 1–12, https://doi.org/10.5772/INTECHOPEN.90227.
[38] E. Tan, İ.M. Kahyaoğlu, S. Karakuş, A sensitive and smartphone colorimetric assay for the detection of hydrogen peroxide based on antibacterial and antifungal matcha extract silver nanoparticles enriched with polyphenol, Polym. Bull. (2021) 1–27, https://doi.org/10.1007/S00289-021-03857-W/TABLES/5.
[39] A.R. Perestrelo, A. Grenha, A.M. Rosa Da Costa, J.A. Belo, Locust bean gum as an alternative polymeric coating for embryonic stem cell culture, Mater. Sci. Eng. C 40 (2014) 336–344, https://doi.org/10.1016/J.MSEC.2014.04.022.
[40] Y. Chen, L. Fu, Y. Duan, Y. Bai, X. Wang, X. Sun, C. Liu, B. Zhang, Z. Di, Effect of organic solvents on the conductivity of polyethylene glycol-based deep eutectic solvents, J. Mol. Liq. 346 (2022), 117038, https://doi.org/10.1016/J.MOLLIQ.2021.117038.
[41] M. Lickmichand, C.S. Shaji, N. Valarmathi, A.S. Benjamin, R.K.Arun Kumar, S. Nayak, R. Saraswathy, S. Sumathi, N.Arunai Nambi Raj, In vitro biocompatibility and hyperthermia studies on synthesized cobalt ferrite nanoparticles encapsulated with polyethylene glycol for biomedical applications, Mater. Today Proc. 15 (2019) 252–261, https://doi.org/10.1016/J.MATPR.2019.05.002.
[42] T. Carpenter, J. Konig, J. Hochfelder, S. Siegel, M. Gans, Polyethylene glycol and polysorbate testing in 12 patients before or after coronavirus disease 2019 vaccine administration, Ann. Allergy Asthma Immunol. 128 (2022) 99–101, https://doi.org/10.1016/J.ANAI.2021.10.009.
[43] A. Abbas, H.M.A. Amin, Silver nanoparticles modified electrodes for electroanalysis: an updated review and a perspective, Microchem. J. 175 (2022), 107166, https://doi.org/10.1016/J.MICROC.2021.107166.
[44] H.M. Soe, A. Abd Manaf, A. Matsuda, M. Jaafar, Performance of a silver nanoparticles-based polydimethylsiloxane composite strain sensor produced using different fabrication methods, Sensors Actuators A Phys. 329 (2021), 112793, https://doi.org/10.1016/J.SNA.2021.112793.
[45] T. Hanawa, Overview of metals and applications, Met. Biomed. Devices (2019) 3–29, https://doi.org/10.1016/B978-0-08-102666-3.00001-8.
[46] J. Wilson, Metallic biomaterials, in: Fundam. Biomater. Met, 2018, pp. 1–33, https://doi.org/10.1016/B978-0-08-102205-4.00001-5.
[47] M. Kumar, R. Kumar, S. Kumar, Coatings on orthopedic implants to overcome present problems and challenges: a focused review, Mater. Today Proc. 45 (2021) 5269–5276, https://doi.org/10.1016/J.MATPR.2021.01.831.
[48] H. Qian, M. Li, Z. Li, Y. Lou, L. Huang, D. Zhang, D. Xu, C. Du, L. Lu, J. Gao, Mussel-inspired superhydrophobic surfaces with enhanced corrosion resistance and dual-action antibacterial properties, Mater. Sci. Eng. C 80 (2017) 566–577, https://doi.org/10.1016/J.MSEC.2017.07.002.
[49] Aminatun, I.A. Furqon, D. Hikmawati, C.A.C. Abdullah, Antibacterial properties of silver nanoparticle (AgNPs) on stainless steel 316L, Nanomed. Res. J. 6 (2021) 117–127, https://doi.org/10.22034/NMRJ.2021.02.004.
[50] L. He, D. Dai, L. Xie, Y. Chen, C. Zhang, Biological effects, applications and strategies of nanomodification of dental metal surfaces, Mater. Des. 207 (2021), 109890, https://doi.org/10.1016/J.MATDES.2021.109890.
[51] R. Apak, K. Güçlü, M. Özyürek, S.E. Karademir, Novel Total antioxidant capacity index for dietary polyphenols and vitamins C and E, using their cupric ion reducing capability in the presence of neocuproine: CUPRAC method, J. Agric. Food Chem. 52 (2004) 7970–7981, https://doi.org/10.1021/JF048741X.
[52] M.B. Arnao, A. Cano, M. Acosta, The hydrophilic and lipophilic contribution to total antioxidant activity, Food Chem. 73 (2001) 239–244, https://doi.org/10.1016/S0308-8146(00)00324-1.
[53] S. Karakuş, N. Taşaltın, C. Taşaltın, N.B. Üllen, Synthesis and characterization of konjac gum/polyethylene glycol-silver nanoparticles and their potential application as a colorimetric sensor for hydrogen peroxide, J. Inorg. Organomet. Polym. Mater. 1 (2021) 1–14, https://doi.org/10.1007/S10904-021-01984-5.
[54] M. Gomathi, P.V. Rajkumar, A. Prakasam, K. Ravichandran, Green synthesis of silver nanoparticles using Datura stramonium leaf extract and assessment of their antibacterial activity, Resour. Technol. 3 (2017) 280–284, https://doi.org/10.1016/J.REFFIT.2016.12.005.
[55] K. Mallikarjuna, N.John Sushma, G. Narasimha, L. Manoj, B.Deva Prasad Raju, Phytochemical fabrication and characterization of silver nanoparticles by using Pepper leaf broth, Arab. J. Chem. 7 (2014) 1099–1103, https://doi.org/10.1016/J.ARABJC.2012.04.001.
[56] R. Sowbarnika, S. Anhuradha, B. Preetha, Enhanced antimicrobial effect of yeast mediated silver nanoparticles synthesized from baker's yeast, Int. J. Nanosci. Nanotechnol. 14 (2018) 33–42.
[57] S. Zainab, S. Hamid, S. Sahar, N. Ali, Fluconazole and biogenic silver nanoparticles-based nano-fungicidal system for highly efficient elimination of multi-drug resistant Candida biofilms, Mater. Chem. Phys. 276 (2022), 125451, https://doi.org/10.1016/J.MATCHEMPHYS.2021.125451.
[58] A.K. Mohamedkhair, Q.A. Drmosh, Z.H. Yamani, Silver nanoparticle-decorated tin oxide thin films: synthesis, characterization, and hydrogen gas sensing, Front. Mater. 6 (188) (2019) 1–10, https://doi.org/10.3389/FMATS.2019.00188/BIBTEX.
[59] A. Mumtaz Hamdani, I. Ahmed Wani, Guar and locust bean gum: composition, total phenolic content, antioxidant and antinutritional characterisation 11 (2017) 53–59, https://doi.org/10.1016/J.BCDF.2017.07.004.
[60] H. Fidan, S. Stankov, N. Petkova, Z. Petkova, A. Iliev, M. Stoyanova, T. Ivanova, N. Zhelyazkov, S. Ibrahim, A. Stoyanova, S. Ercisli, Evaluation of chemical composition, antioxidant potential and functional properties of carob (Ceratonia siliqua L.) seeds, J. Food Sci. Technol. 57 (2020) 2404–2413, https://doi.org/10.1007/S13197-020-04274-Z.
[61] C. Castro-López, C. Espinoza-González, R. Ramos-González, V.D. Boone-Villa, M. A. Aguilar-González, G.C.G. Martínez-Ávila, C.N. Aguilar, J.M. Ventura-Sobrevilla, Spray-drying encapsulation of microwave-assisted extracted polyphenols from Moringa oleifera: influence of tragacanth, locust bean, and carboxymethyl-cellulose formulations, Food Res. Int. 144 (2021), 110291, https://doi.org/10.1016/J.FOODRES.2021.110291.
[62] E. Niki, N. Noguchi, Evaluation of antioxidant capacity. What capacity is being measured by which method? IUBMB Life 50 (2000) 323–329, https://doi.org/10.1080/713803736.
[63] M. Soloviev, A. Gedanken, Coating a stainless steel plate with silver nanoparticles by the sonochemical method, Ultrason. Sonochem. 18 (2011) 356–362, https://doi.org/10.1016/J.ULTSONCH.2010.06.015.
[64] S. Calderon Velasco, A. Cavaleiro, S. Carvalho, Functional properties of ceramic-Ag nanocomposite coatings produced by magnetron sputtering, Prog. Mater. Sci. 84 (2016) 158–191, https://doi.org/10.1016/J.PMATSCI.2016.09.005.
[65] S. Afewerki, N. Bassous, S. Harb, C. Palo-Nieto, G.U. Ruiz-Esparza, F.R. Marciano, T.J. Webster, A.S.A. Furtado, A.O. Lobo, Advances in dual functional antimicrobial and osteoinductive biomaterials for orthopaedic applications, Nanomedicine: NBM 24 (2020), 102143, https://doi.org/10.1016/J.NANO.2019.102143.
[66] A.P.R. Alves Claro, R.T. Konatu, A.L.do A. Escada, M.C. de Souza Nunes, C. V. Maurer-Morelli, M.F. Dias-Netipanyj, K.C. Popat, D. Mantovani, Incorporation of silver nanoparticles on Ti7.5Mo alloy surface containing TiO2 nanotubes arrays for promoting antibacterial coating – in vitro and in vivo study, Appl. Surf. Sci. 455 (2018) 780–788, https://doi.org/10.1016/J.APSUSC.2018.05.189.
[67] A. Liguori, M.E. Gino, S. Panzavolta, P. Torricelli, M. Maglio, A. Parrilli, C. Gualandi, C. Griffoni, G. Barbanti Brodano, M. Fini, M.L. Focarete, Tantalum nanoparticles enhance the osteoinductivity of multiscale composites based on poly (lactide-co-glycolide) electrospun fibers embedded in a gelatin hydrogel, Mater. Today Chem. 24 (2022), 100804, https://doi.org/10.1016/J.MTCHEM.2022.100804.
[68] T. Albrektsson, A. Wennerberg, Oral implant surfaces: part 1–review focusing on topographic and chemical properties of different surfaces and in vivo responses to them, Int. J. Prosthodont. 17 (2004) 536–543.
[69] D. Wojcieszak, M. Mazur, D. Kaczmarek, P. Mazur, B. Szponar, J. Domaradzki, L. Kepinski, Influence of the surface properties on bactericidal and fungicidal activity of magnetron sputtered Ti–Ag and Nb–Ag thin films, Mater. Sci. Eng. C 62 (2016) 86–95, https://doi.org/10.1016/J.MSEC.2016.01.029.
[70] M.V. Roldán, Y. Castro, N. Pellegri, A. Durán, Enhanced photocatalytic activity of mesoporous SiO2/TiO2 sol–gel coatings doped with Ag nanoparticles, J. Sol-Gel Sci. Technol. 76 (2015) 180–194, https://doi.org/10.1007/s10971-015-3765-6.
[71] S.M. Emarati, M. Mozammel, Efficient one-step fabrication of superhydrophobic nano-TiO2/TMPSi ceramic composite coating with enhanced corrosion resistance on 316L, Ceram. Int. 46 (2020) 1652–1661, https://doi.org/10.1016/J.CERAMINT.2019.09.137.
[72] J.-K. Du, C.-Y. Chao, L.-L. Wei, C.-H. Wang, J.-H. Chen, K.-K. Chen, R.-B. Huang, C. Du, J.-K. Chao, C.-Y. Wei, L.-L. Wang, C.-H. Chen, J.-H. Chen, K.-K. Huang, Effects of Ag-rich nano-precipitates on the antibacterial properties of 2205 duplex stainless steel, Metals 11 (2020) 1–14, https://doi.org/10.3390/MET11010023.
[73] R. Chen, H. Ni, H. Zhang, G. Yue, W. Zhan, P. Xiong, A preliminary study on antibacterial mechanisms of silver ions implanted stainless steel, Vacuum 89 (2013) 249–253, https://doi.org/10.1016/J.VACUUM.2012.05.025.
[74] I. Mutlu, Characterisation of localised corrosion behaviour of Ti-Ta-Mo alloy for the nuclear industry, Corros. Rev. 35 (2017) 13–21, https://doi.org/10.1515/CORRREV-2016-0051/MACHINEREADABLECITATION/RIS.